CRISES CASCADES WITHIN ROBUST CHAOS IN PIECEWISE-SMOOTH MAPS

Viktor Avrutin, Michael Schanz
Institute of Parallel and Distributed Systems (IPVS), University of Stuttgart, Germany
{Viktor.Avrutin, Michael.Schanz}@informatik.uni-stuttgart.de

Abstract
This article describes a novel bifurcation phenomenon occurring in the 2D parameter space of piecewise-linear maps. In the region of chaotic behavior we detect an infinite number of interior crises bounding the regions of multi-band attractors. This phenomenon, denoted as bandcount adding scenario, leads to a self-similar structure of the chaotic region in the parameter space.

Key words
multi-band chaotic attractors, bandcount adding, bandcount doubling, interior crises, piecewise-linear maps, discontinuous maps

1 Introduction

One of the phenomena often observed when dealing with piecewise-smooth systems is the so-called robust chaos. In the pioneer work by Banerjee, Yorke and Grebogi (Banerjee *et al.*, 1998) this term is defined by the absence of periodic windows. This means, that an infinitesimally small parameter perturbation does not affect the chaotic nature of the attractor. It was initially assumed, that chaos without periodic windows is not possible for maps with a smooth system function (Barreto *et al.*, 1997; Banerjee *et al.*, 1998). However, some years later it was shown, that it is possible to design smooth maps demonstrating this phenomenon (Andrecut and Ali, 2001*a*; Andrecut and Ali, 2001*b*).

However, the absence of periodic windows does not exclude possible non-smooth changes of the topological structure and geometrical properties of the chaotic attractors caused by infinitesimally small parameter perturbations. Therefore it is less restrictive than a general definition for robustness of attractors. Following the famous work by Milnor "On the concept of attractor" (Milnor, 1985), an attractor $\mathcal{A}$ existing at the point p in parameter space is called robust (structurally stable), iff for all attractors $\mathcal{A}'$ existing at the points $p' \in U_\varepsilon(p)$ in the infinitesimally small neighborhood $U_\varepsilon(p)$ there exists a smooth mapping between $\mathcal{A}$ and $\mathcal{A}'$. This definition means, that an infinitesimally small parameter perturbation does not affect the topological structure and geometrical properties of the attractor. Typically, the chaotic nature of the attractor is preserved as well.

One situation where the difference between both definitions becomes considerably is given by specific chaos-chaos transitions, in particular interior and merging crises. These bifurcations are well-known since the fundamental publications (Grebogi *et al.*, 1982; Grebogi *et al.*, 1983) and investigated in several works theoretically and experimentally (see for instance (Grebogi *et al.*, 1986; Ditto *et al.*, 1989)). Both in smooth and in piecewise-smooth systems interior and merging crises are caused by collisions of a chaotic attractor with an unstable periodic orbit located within its basin of attraction. The attractor at the bifurcation point is robust in the sense of (Banerjee *et al.*, 1998), since there are no periodic windows in its vicinity. However, it is not robust in the sense of (Milnor, 1985), since its geometrical shape and often also the topology (especially the number of bands or strongly connected components) changes at the bifurcation point.

In contrast to individual crisis bifurcations complete bifurcation scenarios formed by several types of crises are still insufficiently investigated. Especially when dealing with piecewise-smooth systems, it is well-known that in the region of robust chaos one-band attractors are often interrupted by small windows containing multi-band attractors. The boundaries of the regions of multi-band attractors are formed by crises bifurcations. Therefore, in this work we will demonstrate how the region of robust chaos is structured and report some novel bifurcation scenarios representing well-organized infinite sequences of crisis bifurcations causing observed self-similarity of these structures.

2 Bandcount adding

Let us consider the following map

$$x_{n+1} = \begin{cases} f_\ell(x) = ax_n + \mu + 1 & \text{if } x_n < 0 \\ f_r(x) = ax_n + \mu - 1 & \text{if } x_n > 0 \end{cases} \quad (1)$$

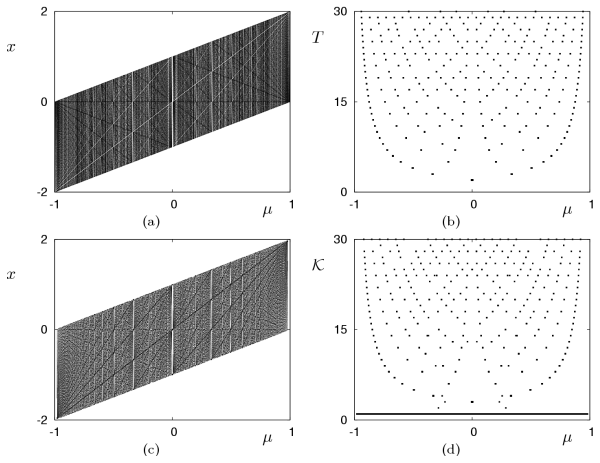

Figure 1. Period adding at $a = 0.99$ (a,b) vs. bandcount adding at $a = 1.01$ (c,d). Although the bifurcation diagrams (a, c) look very similar, all attractors in (a) are periodic, whereas all attractors in (c) are chaotic. Hereby both the periods of the periodic attractors (b) and the bandcounts of the chaotic attractors (d) show the characteristic adding structure.

with $a > 0$, $|\mu| < 1$, representing a common model of a Σ/Δ modulator investigated for instance in (Feely and Chua, 1991; Feely, 1992; Jacomet *et al.*, 2004) and occurring also in biology (Coutinho *et al.*, 2006) as a specific model of genetic regulatory networks. Since the stability of orbits in this system is determined by the slope a only, this system shows for $a < 1$ periodic (and in limiting cases aperiodic non-chaotic) dynamics. For $a > 1$ the dynamics is chaotic in the region $\mathcal{P}_{\text{ch}}$ bounded by the curves of boundary crises $\chi^{\ell/r} = \{(a, \mu) \mid \mu = \pm(a-2)/a\}$ and outside of this region divergent (see Fig. 2). Since no stable periodic orbits for $a > 1$ are possible, the chaotic behavior in the region $\mathcal{P}_{\text{ch}}$ is robust.

In order to detect, which crisis bifurcations occur within $\mathcal{P}_{\text{ch}}$, we have firstly to determine, which unstable periodic orbits exist in this region. Although this question is in general difficult to solve, the first step hereby is to consider the orbits, which are stable within the periodic domain and become unstable at its boundary. In the following a periodic orbit is characterized by the sequence σ consisting of symbols $\mathcal{L}$ (for a point $x < 0$) and $\mathcal{R}$ (for $x > 0$) and representing exactly one period. The orbit corresponding to such a sequence σ will be denoted as O_σ. The region in the parameter space, where O_σ is stable (unstable), is denoted as $\mathcal{P}^s_\sigma$ (respectively $\mathcal{P}^u_\sigma$). These regions are bounded by the curves of border collision bifurcation, where the corresponding orbit O_σ will be destroyed as it collides with the border $x = 0$. These curves are denoted as $\xi^{i,d}_\sigma$, whereby the index $i \in [0, |\sigma|]$ refers to the fact, that the ith point of the orbit collides with the border $x = 0$. The symbol $d \in \{\ell, r\}$ represents the direction of the collision, i.e. whether the ith point of the orbit O_σ collides with the border from the left side or from the right side.

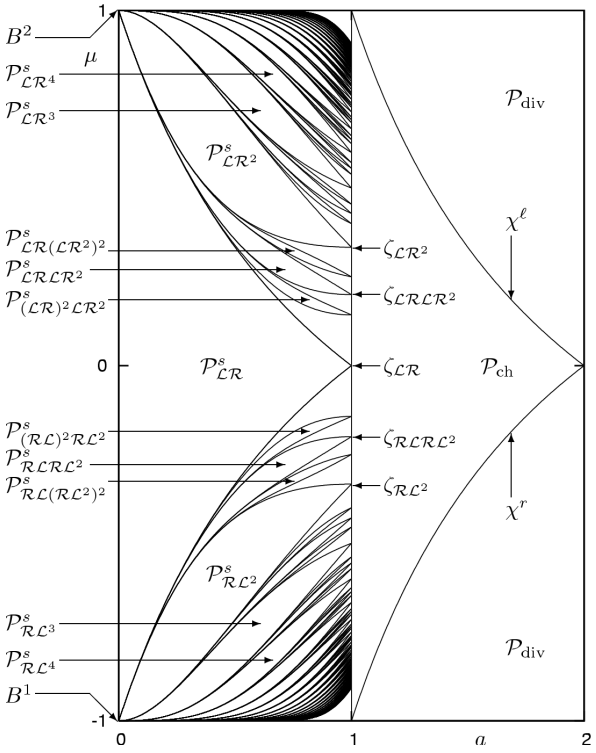

Figure 2. Analytically determined regions of periodic dynamics for orbits up to the third generation of the infinite symbolic sequence adding scheme, as well as regions of chaotic $\mathcal{P}_{\text{ch}}$ and divergent $\mathcal{P}_{\text{div}}$ behavior.

It is shown in (Avrutin *et al.*, 2007), that the structure of the region $\Pi = \{(a, \mu) \mid a < 1\}$ is completely determined by two codimension 2 big bang bifurcations (Avrutin and Schanz, 2006) of the period adding type, which occur at the points $B^1 = (0, -1)$ and $B^2 = (0, 1)$. From each of these points an infinite number of regions $\mathcal{P}^s_\sigma$ originate (see Fig. 2), whereby the sequence σ may be $\mathcal{LR}^n$ or $\mathcal{RL}^n$ with $n = 1, 2, \ldots$. These sequences are denoted in the following as basic sequences, and the corresponding orbits $O_{\mathcal{LR}^n}$ and $O_{\mathcal{RL}^n}$ as basic orbits. Due to the symmetry property $((a, \mu) \to (a, -\mu)) \Rightarrow (x \to -x)$, it is sufficient to consider only one family of basic orbits, for instance $O_{\mathcal{LR}^n}$, since $(a, \mu) \in \mathcal{P}^{s/u}_{\mathcal{LR}^n} \Rightarrow (a, -\mu) \in \mathcal{P}^{s/u}_{\mathcal{RL}^n}$. Note that we use here and in the following a compact notation: for instance $\mathcal{P}^{s/u}_\sigma$ refers to the two different objects, namely $\mathcal{P}^s_\sigma$ and $\mathcal{P}^u_\sigma$. The boundaries of the existence regions of a basic orbit (the curves of border collision bifurcations $\xi^{0,\ell/n,r}_{\mathcal{LR}^n}$ and $\xi^{n,\ell/0,r}_{\mathcal{RL}^n}$ respectively) can be calculated analytically for arbitrary n. It can be shown, that for each n the region $\mathcal{P}^s_{\mathcal{LR}^n}$ originates from the big bang bifurcation point B^2 and collapses to a singular point $\zeta_{\mathcal{LR}^n} = (1, (n-1)/(n+1)) \in \partial\Pi$ located at the boundary of the region Π (line $a = 1$) where the orbit $O_{\mathcal{LR}^n}$ becomes unstable. For $a > 1$ all these unstable orbits still exist, and the same border collision bifurcations curves $\xi^{0,\ell/n,r}_{\mathcal{LR}^n}$ are confining now the regions $\mathcal{P}^u_{\mathcal{LR}^n}$. Remarkably the regions $\mathcal{P}^s_{\mathcal{LR}^n}$ and $\mathcal{P}^s_{\mathcal{RL}^n}$ do not completely cover the region Π. Namely, between

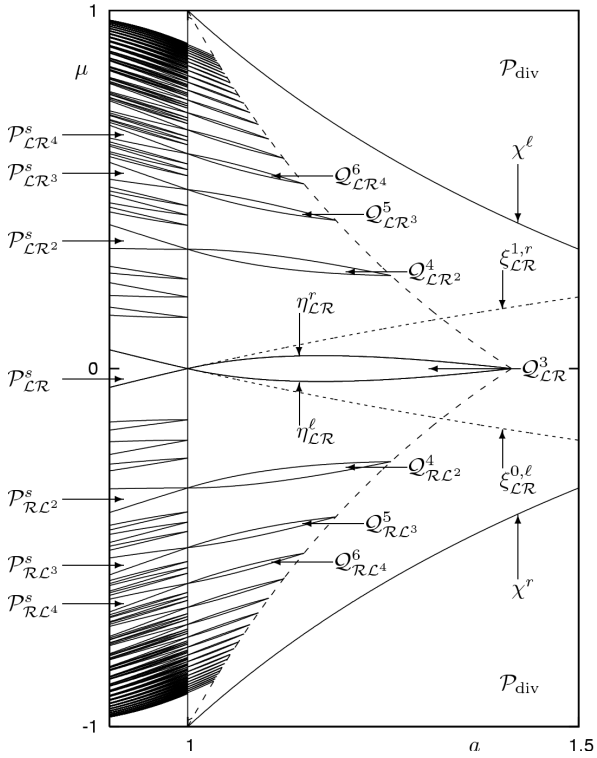

Figure 3. Analytically calculated regions $\mathcal{Q}^{n+2}_{\mathcal{LR}^n}$ and $\mathcal{Q}^{n+2}_{\mathcal{RL}^n}$ ($n \leq 10$) of multi-band attractors caused by the basic orbits. For the unstable two-periodic orbit $O^u_{\mathcal{LR}}$ the existence boundaries (border collision curves $\xi^{1,r/0,\ell}_{\mathcal{LR}}$) are shown, as well as the curves of interior crises $\eta^{r/\ell}_{\mathcal{LR}}$, caused by this orbit.

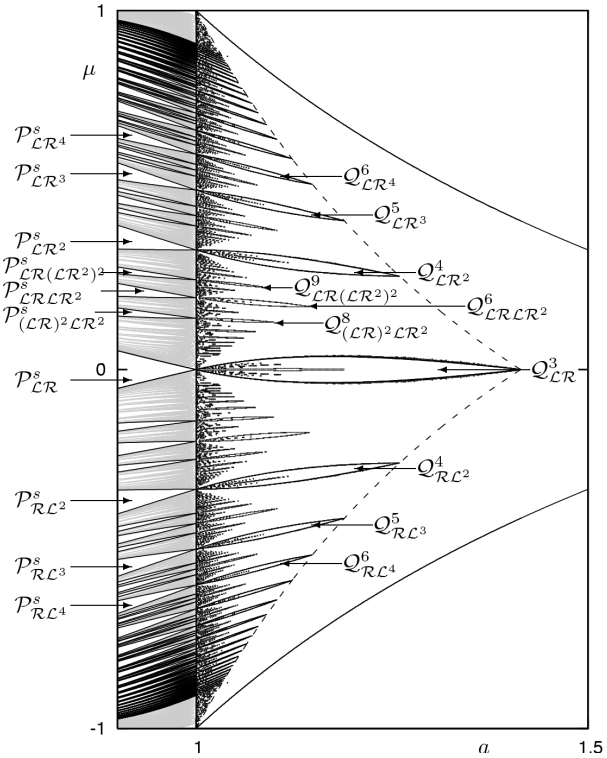

Figure 4. Numerically detected regions $\mathcal{Q}^{\mathcal{K}}_\sigma$ of multi-band attractors. Marked are some of the regions corresponding to the first, second and third generations of the bandcount adding scenario. Note the correspondence between the period adding scenario for $a < 1$ and the bandcount adding scenario for $a > 1$.

each two subsequent regions $\mathcal{P}^s_{\mathcal{LR}^n}$ and $\mathcal{P}^s_{\mathcal{LR}^{n+1}}$ there is some "free space", where an infinite number of regions $\mathcal{P}^s_\sigma$ are located, whereby the specific sequences σ can be obtained from a pair of basic sequences $\mathcal{LR}^n$ and $\mathcal{LR}^{n+1}$ using the infinite sequence adding scheme (Avrutin *et al.*, 2006). This sequence adding scheme is a symbolic representation of the well-known Farey tree (Lagarias and Tresser, 1995; Bai-Lin, 1989) also known as Stern-Brocot tree and implies that between the regions $\mathcal{P}^s_{\mathcal{LR}^n}$ and $\mathcal{P}^s_{\mathcal{LR}^{n+1}}$ there exists the region $\mathcal{P}^s_{\mathcal{LR}^n\mathcal{LR}^{n+1}}$. Furthermore between regions $\mathcal{P}^s_{\mathcal{LR}^n}$ and $\mathcal{P}^s_{\mathcal{LR}^n\mathcal{LR}^{n+1}}$ the region $\mathcal{P}^s_{(\mathcal{LR}^n)^2\mathcal{LR}^{n+1}}$ and between regions $\mathcal{P}^s_{\mathcal{LR}^n\mathcal{LR}^{n+1}}$ and $\mathcal{P}^s_{\mathcal{LR}^{n+1}}$ the region $\mathcal{P}^s_{\mathcal{LR}^n(\mathcal{LR}^{n+1})^2}$ exists and so on. Hereby the basic sequences occur always in the first layer of the sequence adding scheme, the sequences $\mathcal{LR}^n\mathcal{LR}^{n+1}$ in its second layer, the sequences $(\mathcal{LR}^n)^2\mathcal{LR}^{n+1}$ and $\mathcal{LR}^n(\mathcal{LR}^{n+1})^2$ in the third layer and so on. According to this we denote the layer of the sequence adding scheme, where a specific sequence σ is generated, as the generation of this sequence and of the corresponding orbit O_σ. For instance, in Fig. 2 the analytically calculated regions $\mathcal{P}^s_\sigma$ are shown for the orbits O_σ of the generations one, two and three. Remarkably, the existence regions of all orbits O_σ have similar structure. For each σ the regions $\mathcal{P}^s_\sigma$ and $\mathcal{P}^u_\sigma$ collapse to the point $\zeta_\sigma \in \partial\Pi$.

In the region $\mathcal{P}_{\rm ch}$ each of the orbits O_σ described above is unstable and leads to two interior crises η^ℓ_σ and η^r_σ. These curves can be calculated analytically using the condition that the points of the kneading orbits $f^{[k]}(f_\ell(0))$ and $f^{[k]}(f_r(0))$ collides for some k with the involved unstable periodic orbit. In other words, at the crisis bifurcation the discontinuity point $x = 0$ belongs to the stable manifold of the involved unstable periodic orbit. The resulting structure of the region $\mathcal{P}_{\rm ch}$ is shown in Fig. 3, where the regions $\mathcal{Q}^{|\sigma|+1}_\sigma$ bounded by the curves $\eta^{r/\ell}_\sigma$ are marked for $\sigma = \mathcal{LR}^n$ and $\sigma = \mathcal{RL}^n$. The following properties of the crisis curves $\eta^{\ell/r}_\sigma$ are important:

1. The multi-band attractors undergoing crises at the bifurcation curves $\eta^{\ell/r}_\sigma$ where an orbit with period $|\sigma|$ is involved in have $|\sigma| + 1$ bands. That means, before the crisis the attractor has $|\sigma|$ gaps and in each gap one point of the unstable periodic orbit is located.
2. Obviously, each region $\mathcal{Q}^{|\sigma|+1}_\sigma$ bounded by the curves $\eta^{\ell/r}_\sigma$ is embedded into the region $\mathcal{P}^u_\sigma$, where the unstable orbit responsible for the crisis exists.
3. The $\eta^{\ell/r}_\sigma$ curves originate from the point ζ_σ, from which the region $\mathcal{P}^u_\sigma$ originates as well. At this point the boundaries of the region $\mathcal{Q}^{|\sigma|+1}_\sigma$ are tangent with the boundaries of the region $\mathcal{P}^u_\sigma$.

Especially the properties (2) and (3) imply that in

the parameter space the regions $\mathcal{Q}_\sigma^{|\sigma|+1}$ are arranged in the same order as the regions $\mathcal{P}_\sigma^u$ and also as the regions $\mathcal{P}_\sigma^s$ for $a < 1$. For instance, for each n between the regions $\mathcal{Q}_{\mathcal{LR}^n}^{n+2}$ and $\mathcal{Q}_{\mathcal{LR}^{n+1}}^{n+3}$ there exists the region $\mathcal{Q}_{\mathcal{LR}^n\mathcal{LR}^{n+1}}^{2n+4}$. Similarly, between the regions $\mathcal{Q}_{\mathcal{LR}^n}^{n+2}$ and $\mathcal{Q}_{\mathcal{LR}^n\mathcal{LR}^{n+1}}^{2n+4}$ there is the region $\mathcal{Q}_{(\mathcal{LR}^n)^2\mathcal{LR}^{n+1}}^{3n+5}$, whereas between the regions $\mathcal{Q}_{\mathcal{LR}^n\mathcal{LR}^{n+1}}^{2n+4}$ and $\mathcal{Q}_{\mathcal{LR}^{n+1}}^{n+3}$ the region $\mathcal{Q}_{\mathcal{LR}^n(\mathcal{LR}^{n+1})^2}^{3n+6}$ can be found. Examples for these regions are presented in Fig. 4. This figure shows the numerically calculated regions of periodic dynamics (for $a < 1$) and the regions of multi-band attractors (for $a > 1$). As one can see, both structures are organized by the same principles. This is the reason, why we denote the structure formed by multi-band attractors in the region Π as *bandcount adding*, similar to the period adding structure existing for $a < 1$.

However, numerical experiments demonstrate that the correspondence between both structures mentioned above is not one-to-one. In fact within each region $\mathcal{Q}_\sigma^{|\sigma|+1}$ involved into the bandcount adding scenario fine substructures can be detected, consisting of regions with higher bandcounts. The existence of these regions can not be explained based on the periodic orbits of the period adding structure for $a < 1$. Instead we have to consider the orbits which are nowhere stable (denoted in the following as pure unstable orbits).

Let us consider as an example the family of regions $\mathcal{Q}_{\mathcal{LR}^n}^{n+2}$, which belong to the first generation of the bandcount adding scenario. Along the middle line of each region $\mathcal{Q}_{\mathcal{LR}^n}^{n+2}$ we observe a sequence of regions $\mathcal{Q}_{\sigma_i^n}^{\mathcal{K}_i^n}$ with bandcounts

$$\mathcal{K}_i^n = 1 + (n+1) \cdot \sum_{k=0}^{i-1} 2^k = 1 + (2^i - 1)(n+1)$$

The boundaries of these regions are defined by interior crises caused by unstable periodic orbits with doubled periods. For instance, the sequence of regions with bandcounts 7, 15, 31 ..., (see Fig. 5) located within the region $\mathcal{Q}_{\mathcal{LR}}^3$ are caused by the pure unstable periodic orbits $O_{\sigma_i^1}^{\mathcal{K}_i^1}$ with $\sigma_1^1 = \mathcal{LR}$, $\sigma_2^1 = \mathcal{L}^2\mathcal{R}^2$, $\sigma_3^1 = \mathcal{L}^2\mathcal{R}\mathcal{L}\mathcal{R}^2\mathcal{L}\mathcal{R}$, $\sigma_4^1 = \mathcal{L}^2\mathcal{R}\mathcal{L}\mathcal{R}^2\mathcal{L}^2\mathcal{R}^2\mathcal{L}\mathcal{R}\mathcal{L}^2\mathcal{R}^2$, and so on. The following properties of these regions are important:

1. The existence areas of all involved pure unstable periodic orbits $O_{\sigma_i^1}^{\mathcal{K}_i^1}$ originate from the same point $\zeta_{\sigma_1^1}$ at the line $a = 1$.
2. The regions $\mathcal{Q}_{\sigma_i^n}^{\mathcal{K}_i^n}$ for increasing i are nested in each other, that means the region $\mathcal{Q}_{\sigma_{i+1}^n}^{\mathcal{K}_{i+1}^n}$ is located within the region $\mathcal{Q}_{\sigma_i^n}^{\mathcal{K}_i^n}$.
3. The multi-band chaotic attractors within the region $\mathcal{Q}_{\sigma_i^n}^{\mathcal{K}_i^n}$ are influenced by all pure unstable periodic orbits $O_{\sigma_j^1}^{\mathcal{K}_j^1}$ with $j = 1..i$, whereby all points of these orbits are located in different gaps of the attractor. That means for instance, that the attractors within the region $\mathcal{Q}_{\sigma_4^n}^{\mathcal{K}_4^n}$ have 16 gaps occupied by the points of the orbit $O_{\sigma_4^1}^{\mathcal{K}_4^1}$, 8 further gaps occupied by the orbit $O_{\sigma_3^1}^{\mathcal{K}_3^1}$, 4 gaps occupied by $O_{\sigma_2^1}^{\mathcal{K}_2^1}$ and 2 gaps occupied by $O_{\sigma_1^1}^{\mathcal{K}_1^1}$. Consequently, the attractors have $16 + 8 + 4 + 2 = 30$ gaps and thus $K_4^1 = 31$ bands.

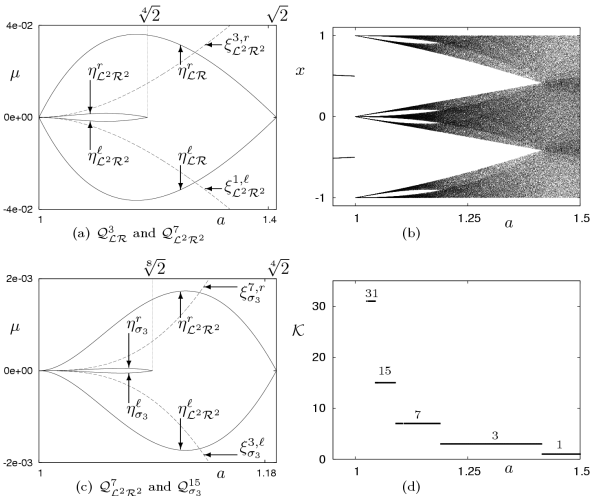

Figure 5. (a) Analytically calculated areas $\mathcal{Q}_{\mathcal{LR}}^3$ and $\mathcal{Q}_{\mathcal{L}^2\mathcal{R}^2}^7$. For the unstable orbit $O_{\mathcal{L}^2\mathcal{R}^2}^u$ the existence boundaries (border collision curves $\xi_{\mathcal{L}^2\mathcal{R}^2}^{1,r/0,\ell}$) are shown, as well as the curves of interior crises $\eta_{\mathcal{L}^2\mathcal{R}^2}^{r/\ell}$, caused by this orbit. (c) Similar results for the orbits $\mathcal{Q}_{\mathcal{L}^2\mathcal{R}^2}^7$ and $\mathcal{Q}_{\mathcal{L}^2\mathcal{R}\mathcal{L}\mathcal{R}^2\mathcal{L}\mathcal{R}}^{15}$. (b) Bifurcation diagram along the line $\mu = 0$ (middle line of all regions involved into the bandcount doubling scenario within $\mathcal{Q}_{\mathcal{LR}}^3$). (d) corresponding bandcount diagram.

Since a sequence of interior crises forming the regions $\mathcal{Q}_{\sigma_i^n}^{\mathcal{K}_i^n}$ is caused by the orbits with doubled periods we denote it as a *bandcount doubling* cascade (although the bandcounts within the cascade are not exact doubled, like it is the case for the periods within a period-doubling cascade). Note that bandcount doubling cascades can be observed in such well-known systems as the logistic map (where it follows each period doubling cascade) and the tent map.

Of course, the same properties hold not only for the regions $\mathcal{Q}_{\mathcal{LR}^n}^{n+2}$ from the first generation of the overall bandcount adding scenario, but for the regions involved in all further generations as well.

Next let us consider the interior structure of the regions $\mathcal{Q}_\sigma^{|\sigma|+1}$ involved into the bandcount adding scenario beneath their middle curves. For simplicity we will proceed with the already mentioned example, namely with the region $\mathcal{Q}_{\mathcal{LR}}^3$, keeping in the mind that the results we discuss are valid for all regions $\mathcal{Q}_\sigma^{|\sigma|+1}$. As shown in Fig. 6.(a), varying the parameters along an arc around the point $\zeta_{\mathcal{LR}}$ within the region $\mathcal{Q}_{\mathcal{LR}}^3$ we observe a large number of intervals with bandcounts greater than three. The scan curve in the parameter space we con-

sider here is given by the elliptic arc $a = 1 + R_a \sin\varphi$, $\mu = R_\mu \cos\varphi$ around the point $\zeta_{\mathcal{LR}}$ with $R_a = 0.05$ and $R_\mu = 0.005$. For φ between approximately -80 and 80 degrees this arc is located within the region $\mathcal{Q}^3_{\mathcal{LR}}$, whereby the used value $\sqrt[8]{2} < 1+R_a < \sqrt[4]{2}$ implies, that the scan curve we use intersects the regions $\mathcal{Q}^7_{\sigma_2^1} \equiv \mathcal{Q}^7_{\mathcal{L}^2\mathcal{R}^2}$ and $\mathcal{Q}^{15}_{\sigma_3^1}$ but does not intersect $\mathcal{Q}^{31}_{\sigma_4^1}$ and any further regions forming the bandcount doubling cascade described above. Consequently, in the middle part of Fig. 6 we observe the bandcounts 7 and 15 but do not observe the bandcounts 31, 63, and so on. In Fig. 6.(b) the corresponding bifurcation diagram is presented, whereby for the sake of clarity we show as blowups only that parts of the state space where the points of the attractors are located, and the large gaps in between are skipped.

Straight forward calculation shows that within the region $\mathcal{Q}^3_{\mathcal{LR}}$ above the region $\mathcal{Q}^7_{\mathcal{L}^2\mathcal{R}^2}$ there exists a sequence of regions $\mathcal{Q}^{2n+7}_{\mathcal{L}^2\mathcal{R}^2(\mathcal{LR})^n}$, and below the region $\mathcal{Q}^7_{\mathcal{L}^2\mathcal{R}^2}$ a sequence of regions $\mathcal{Q}^{2n+7}_{\mathcal{R}^2\mathcal{L}^2(\mathcal{RL})^n}$ with the following properties:

1. Each of these regions originates from the point $\zeta_{\mathcal{LR}}$.
2. The bandcounts in these regions are explained by by $2n+4$ gaps where the points of the responsible unstable orbit $O_{\mathcal{R}^2\mathcal{L}^2(\mathcal{RL})^n}$ are located in, and two further gaps containing the points of the orbit $O_{\mathcal{LR}}$.
3. Like the regions $\mathcal{Q}^{n+2}_{\mathcal{LR}^n}$ and $\mathcal{Q}^{n+2}_{\mathcal{RL}^n}$ also the regions $\mathcal{Q}^{2n+7}_{\mathcal{L}^2\mathcal{R}^2(\mathcal{LR})^n}$ and $\mathcal{Q}^{2n+7}_{\mathcal{R}^2\mathcal{L}^2(\mathcal{RL})^n}$ represent the first generation of the bandcount adding scheme. Therefore, between each two consequent regions $\mathcal{Q}^{2n+7}_{\mathcal{L}^2\mathcal{R}^2(\mathcal{LR})^n}$ and $\mathcal{Q}^{2n+9}_{\mathcal{L}^2\mathcal{R}^2(\mathcal{LR})^{n+1}}$ there is a region of attractors with $4n+13$ bands, whereby the periodic orbit causing the interior crises of these attractors is $O_{\mathcal{L}^2\mathcal{R}^2(\mathcal{LR})^n\mathcal{L}^2\mathcal{R}^2(\mathcal{LR})^{n+1}}$. These regions belong to the second generation of the bandcount adding scenario within the region $\mathcal{Q}^3_{\mathcal{LR}}$, and so on. All these regions originate also from the point $\zeta_{\mathcal{LR}}$.

As one can see, in each from the infinite number of the regions involved into the bandcount adding scenario caused by unstable basic orbits a further bandcount adding scenario caused by pure unstable orbits is nested. This nested bandcount adding scenario involves a further infinite number of regions. The most striking fact is, that this nesting process continues ad infinitum, leading to a self-similarity of the parameter space. Especially, along the middle line of each region $\mathcal{Q}^{\mathcal{K}}_{\sigma}$ we observe the bandcount doubling cascade caused by the orbits with periods $2^i|\sigma|$. The bandcounts of the involved regions have the form

$$\mathcal{K}_i = (\mathcal{K} - |\sigma|) + |\sigma| \cdot \sum_{k=0}^{i-1} 2^k = \mathcal{K} + |\sigma|(2^i - 2)$$

In other words, in the middle of each region $\mathcal{Q}^{\mathcal{K}}_{\sigma}$ (with

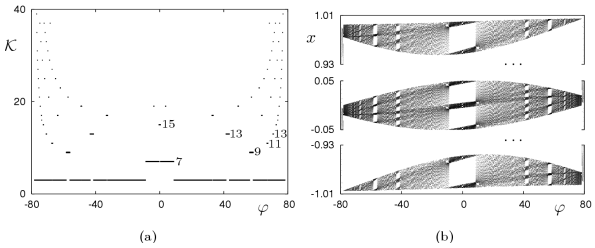

Figure 6. Numerically determined bifurcation scenario within the region $\mathcal{Q}^3_{\mathcal{LR}}$. Shown are bandcounts (a) and bifurcation diagram (b) along the elliptic arc around the point $\zeta_{\mathcal{LR}}$ marked in Fig. 7. Labeled are some of the bandcounts described in the text.

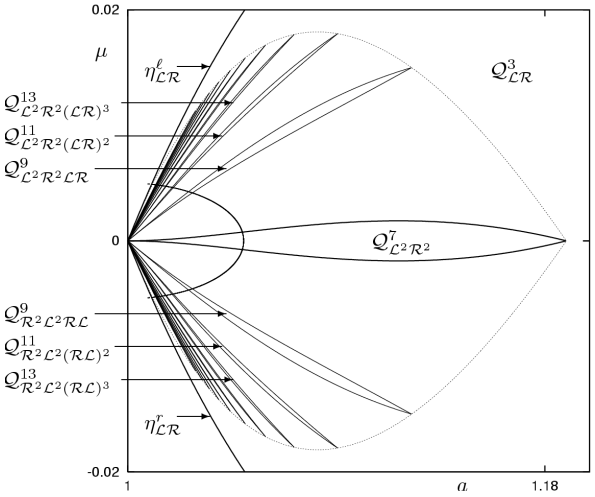

Figure 7. Analytically calculated regions $\mathcal{Q}^{2n+7}_{\mathcal{L}^2\mathcal{R}^2(\mathcal{LR})^n}$ for $n \leq 10$ located within the region $\mathcal{Q}^3_{\mathcal{LR}}$. The elliptic arc marks the scan curve used in the Fig. 6.

$\mathcal{K} \geq |\sigma| + 1$) there is a region $\mathcal{Q}^{\mathcal{K}+2|\sigma|}_{\rho}$. The interior crises leading to this regions are caused by the unstable periodic orbits O_ρ with period $|\rho| = 2|\sigma|$. Within the region $\mathcal{Q}^{\mathcal{K}}_{\sigma}$ and beneath the region $\mathcal{Q}^{\mathcal{K}+2|\sigma|}_{\rho}$ there is a family of regions $\mathcal{Q}^{\mathcal{K}+(n+2)|\sigma|}_{\sigma^n\rho}$, as well as regions $\mathcal{Q}^{\mathcal{K}+|\varpi|}_{\varpi}$, whereby the sequence ϖ can be obtained from a pair $\sigma^n\rho$, $\sigma^{n+1}\rho$ with $n \geq 0$ using the infinite symbolic sequence adding scheme.

Remarkably, the reported scenario lead us to an unexpected conclusion related to the boundary between the regions Π of periodic and $\mathcal{P}_{\text{ch}}$ of chaotic behavior. As already mentioned, at this boundary the points ζ_σ are located, whereby for each periodic orbit O_σ stable within the region Π the region $\mathcal{P}^s_\sigma$ collapses to the singular point ζ_σ. Now we state, that from each of these points an infinite number of regions $\mathcal{P}^s_\rho$ originates, whereby the orbits O_ρ are pure unstable and undergo interior crisis bifurcations within the region $\mathcal{Q}^{|\sigma+1|}_{\sigma}$. Hence, at each of the points ζ_σ an infinite number of border collision bifurcation curves meets, as well as a further infinite number of interior crises curves. According to the notation introduced in (Avrutin and

Schanz, 2006), we conclude that each of these points represents a codimension 2 big bang bifurcation point.

3 Summary

In this paper we considered a piecewise-linear discontinuous map and described the structure of the chaotic region in the 2D parameter space. It was shown, that this region has a complex and presumably self-similar structure caused by interior crises of one- and multi-band chaotic attractors. The overall 2D structure is formed by two specific 1D bifurcation scenarios, namely bandcount adding and bandcount doubling, nested into each other. For both scenarios we demonstrated, which unstable periodic orbits are responsible for their formation. It is especially remarkable, that the first level of the overall bifurcation structure is caused by periodic orbits, which originate from the region of stable periodic dynamics. In contrast to this, all further levels are induced by pure unstable periodic orbits, this means periodic orbits which are unstable for any parameter values. All these results can be summarized by a few rules, which describe the self-similarity of the 2D bifurcation structures and allow to predict the bandcounts of the involved multi-band chaotic attractors up to arbitrary high values. These rules, developed using the map considered in this work, are applicable for a more general class of dynamical systems, showing the phenomenon of robust chaos. Especially the discontinuous 2D normal form map investigated for instance in (Dutta *et al.*, 2006) shows the phenomenon described in this work. Consequently it must also be the case for all systems reducible to this normal form.

Finally, the results of this paper can be seen as a confirmation that the term of robust chaos, must be used carefully, since chaotic attractors which are robust in the sense of (Banerjee *et al.*, 1998) are not necessarily robust in the sense of (Milnor, 1985).

References

Andrecut, M. and M.K. Ali (2001*a*). Example of robust chaos in a smooth map. *Europhys. Lett.* **54**, 300–305.

Andrecut, M. and M.K. Ali (2001*b*). Robust chaos in smooth unimodal maps. *Phys. Rev. E* **64**(2), 025203.

Avrutin, V. and M. Schanz (2006). On multi-parametric bifurcations in a scalar piecewise-linear map. *Nonlinearity* **19**, 531–552.

Avrutin, V., M. Schanz and S. Banerjee (2006). Multi-parametric bifurcations in a piecewise–linear discontinuous map. *Nonlinearity* **19**, 1875–1906.

Avrutin, V., M. Schanz and S. Banerjee (2007). Codimension-3 bifurcations: Explanation of the complex 1-, 2- and 3d bifurcation structures in nonsmooth maps. *Phys. Rev. E*.

Bai-Lin, Hao (1989). *Elementary symbolic dynamics and chaos in dissipative systems*. World Scientific Publishing.

Banerjee, S., J. Yorke and C. Grebogi (1998). Robust chaos. *Phys.Rev.Lett* **80**(14), 3049–3052.

Barreto, E., B.R. Hunt, C. Grebogi and J.A. Yorke (1997). From high dimensional chaos to stable periodic orbits: The structure of parameter space. *Phys. Rev. Lett.* **78**(24), 4561–4564.

Coutinho, R., B. Fernandez, R. Lima and A. Meyroneine (2006). Discrete time piecewise affine models of genetic regulatory networks. *J. Math. Biol.* **52**, 524–570.

Ditto, W. L., S. Rauseo, R. Cawley, C. Grebogi, G.-H. Hsu, E. Kostelich, E. Ott, H. T. Savage, R. Segnan, M. L. Spano and J. A. Yorke (1989). Experimental observation of crisis-induced intermittency and its critical exponent. *Phys. Rev. Lett.* **63**(9), 923–926.

Dutta, P., B. Routroy, S. Banerjee and S. Alam (2006). Border collision bifurcations in n-dimensional piecewise linear discontinuous maps. arXiv:nlin/0601038v2.

Feely, O. (1992). Nonlinear dynamics of sigma-delta modulation. In: *Proc. Midwest Symp. Circuits Syst.*. pp. 760–3.

Feely, O. and L. Chua (1991). The effect of integrator leak in $\Sigma\Delta$ modulation. *IEEE Trans. Circuits Syst.* **38**(11), 1293–1305.

Grebogi, C., E. Ott and J. A. Yorke (1982). Chaotic attractors in crisis. *Phys. Rev. Lett.* **48**(22), 1507–1510.

Grebogi, C., E. Ott and J. A. Yorke (1983). Crisis: sudden changes in chaotic attractors and transient chaos. *Physica* **D 7**, 181.

Grebogi, C., E. Ott and J. A. Yorke (1986). Critical Exponent of Chaotic Transients in Nonlinear Dynamical Systems. *Phys. Rev. Lett.* **57**(11), 1284–1287.

Jacomet, M., J. Goette, V. Zbinden and C. Narvaez (2004). On the dynamic behavior of a novel digital-only sigma-delta A/D converter. In: *Proc. of the 17th symposium on Integrated circuits and system design*. Brazil. pp. 222 – 227.

Lagarias, J.C. and C. Tresser (1995). A walk along the branches of the extended Farey tree. *IBM Jour. of Res. and Dev.* **39**, 283–94.

Milnor, J. (1985). On the Concept of Attractor. *Commun. Math. Phys.* **99**, 177–195.